Available online at www.sciencedirect.com
SCIENCE DIRECT®
ELSEVIER
International Journal of Multiphase Flow 29 (2003) 1719–1747
International Journal of Multiphase Flow
www.elsevier.com/locate/ijmulflow

On the simulation of three-phase slug flow in nearly horizontal pipes using the multi-fluid model

M. Bonizzi, R.I. Issa *

Department of Mechanical Engineering, Imperial College of Science, Technology and Medicine, Exhibition Road, London SW7 2BX, UK

Received 8 January 2003; received in revised form 1 September 2003

Abstract

The article presents a mathematical model to simulate three-phase (liquid/liquid/gas) stratified and slug flows. The approach is based on the one-dimensional transient two-fluid model in which the two-phases consist of the gas and the mixture of the two liquids, with the motion of the liquid phases relative to each other being modelled via a drift–flux model. In order to close the model, a scalar transport equation for the conservation of mass for one of the liquid phases is introduced. Other closure models incorporated relate to the liquid–liquid flow pattern (stratified or fully dispersed), the phase inversion point (when the continuous liquid phase becomes dispersed in the other and vice-versa), the slip between the liquid phases and the mixture viscosity (which changes abruptly when phase inversion occurs). The equations are solved numerically using a previously developed finite volume methodology that had been applied to the prediction of two-phase slug flow and by which liquid slugs are automatically captured as an outcome of the numerical integration. The new method is applied to the study of the flow of oil, water and air in horizontal pipes. The method is shown to be able to predict locally whether the two liquids form a dispersion (of either oil droplets in water continuous flow (O/W) or water droplets in oil continuous flow (W/O)) or flow in stratified layers. It is demonstrated that the developed model is capable of correctly predicting slugging, and is moreover able to reproduce successfully observed experimental trends for the major slug properties, such as pressure gradient, slug frequency, and total liquid hold-up. The study revealed that the slip between the two liquid phases plays a major role in determining the slug characteristics in three-phase flow.

Keywords: Slug flow; Three-phase flow; Liquid–liquid flow pattern; Phase inversion; Drift–flux; Numerical simulation; Two-fluid model

* Corresponding author. Fax: +44-20-78238845.
E-mail address: r.issa@imperial.ac.uk (R.I. Issa).

0301-9322/$ - see front matter
doi:10.1016/j.ijmultiphaseflow.2003.09.002

1. Introduction

Three-phase flow of two liquids and gas occurs often, especially in the production of hydrocarbons from oil and gas fields when oil, water, and natural gas flow in the transporting pipelines. In such environment, a frequently encountered flow pattern is slug flow. The prediction of three-phase gas/liquid/liquid flows is therefore of importance to industry.

Bearing in mind that even two-phase gas–liquid flows are highly complex, it is immediately apparent that the addition of a third phase will substantially add to this complexity. In such flow, physical phenomena additional to those occurring in two-phase flow play a crucial role. A major difference between two and three-phase flow, lies in the fact that in the latter, the presence of two liquids gives rise to a wider variety of flow patterns (Hall, 1997). Depending on the flow rates of the phases, if sufficient mixing takes place, one liquid may be dispersed in the other; otherwise, the liquids will flow in separate layers. Still within the stratified pattern, mixing layers at the liquid–liquid interface may develop in such a way that even the stratified configurations consist of different phase distributions (Açikgöz et al., 1992).

Açikgöz et al. (1992) investigated an oil–water–gas system flowing in a horizontal Plexiglas tube of 5.78 m length and 19 mm internal diameter. The oil used was a North Sea crude, with a dynamic viscosity of $\mu_O = 0.1164$ Pa s, almost 116 times more viscous than the water phase. The superficial velocities ranged between 0.15–50 m/s for the air, 0.043–0.24 m/s for the oil, and 0.004–0.66 m/s for the water. Different flow pattern maps were constructed for different values of the oil superficial velocity U_O. The authors classified the flow patterns according to the combination of the following flow properties: (i) liquid phase that is predominantly in contact with the pipe walls, (ii) liquid–liquid flow pattern (either separated or dispersed), (iii) relevant flow pattern between the liquid (oil + water) and the gas phases. For the first part of their three-phase flow pattern determination, Açikgöz et al. identified either oil based, or water based flows; for the second part dispersed, separated, or separated–dispersed liquid–liquid flow; for the third part they identified six possible patterns: stratified, wavy, plug, slug, annular, and dispersed.

Pan (1996) studied three-phase slug flow experimentally using a pipe made of stainless steel, 38 m long and 77.92 mm internal diameter. The oil used was highly viscous ($\mu_O = 48$ mPa s), almost 50 times more viscous than water. The oil–water surface tension was $\sigma_{OW} = 0.03$ N/m. The flow patterns could be obtained at the end of the test section by visualisation, through an acrylic section, encased in a high pressure tube, using a 24 frame per second video camera that recorded the flow through the acrylic section. The type of classification adopted by Pan (and other subsequent researchers) was to base the flow regimes firstly on the liquid–liquid flow pattern (either fully dispersed or segregated flow), secondly on the identity of the continuous phase in the case of dispersion (either oil or water continuous), and finally on the gas–total liquid (oil + water) flow pattern (bubble, stratified, plug, slug, or annular). The approach is therefore quite similar to that used by Açikgöz et al.

When mixing of the phases takes place, either of the two-phases (oil or water) may be continuous, and the other dispersed (in the form of droplets). Phase inversion, whereby the continuous and dispersed phase spontaneously exchange role, may also occur. Such phenomenon is common, and occurs in a wide range of industrial applications. However, the intricate mechanisms responsible for phase inversion and the effect of physical and geometrical parameters on it

are not well understood yet. Depending on which phase is continuous and which is dispersed, the pressure gradient in either case can be quite different; it is therefore very important to predict the occurrence of phase inversion. When phase inversion takes place, an abrupt change in the frictional pressure drop of the oil–water mixture was observed by investigators, such as Malinowsky (1975), Hall (1992), Pan (1996), and Odozi (2000). This is because the viscosity of the mixture is largely determined by which of the phases is continuous and which is dispersed. For example, Malinowsky (1975) conducted slug flow experiments with low viscosity oils ($\mu_O \approx 4$–5 mPa s) in a horizontal transparent acrylic pipe of length 29.7 m and internal diameter of 38.1 mm, at pressure of 2 bar. The ranges of the superficial velocities employed in the experiments were as follows: 1.5–4.3 m/s for the air, 0.26–1.36 m/s for oil, and 0.19–2.08 m/s for water. The oil–water surface tension was $\sigma_{OW} = 0.023$ N/m. The majority of the flow tests were performed in slug flow, except those for the highest gas velocities in which the observed pattern was between misty annular and slug. Malinowsky (1975) assessed the Beggs and Brill (1973) pressure gradient correlation against his experimental data, supposing that the oil–water mixture had a viscosity obeying linear interpolation between that of the oil and water phases. As the correlation constantly under-predicted his measurements (by up to 50%), Malinowsky (1975) concluded that the linear viscosity approximation for the oil–water mixture was a poor representation. By applying the Beggs and Brill (1973) pressure gradient correlation, he then back calculated the mixture viscosity from the known experimental values of the pressure gradient, and found that the oil–water mixture viscosity can be several times greater than that of the pure liquid phase: in the oil continuous region Malinowsky (1975) found that the mixture viscosity was about 30 times the oil viscosity for a 50% water input fraction.

Odozi (2000) measured the liquid hold-ups in three-phase slug flow using a dual gamma densitometer, while measuring the pressure drop using two pressure transducers mounted close to the pipe exit. The experimental campaigns were mainly made for a horizontal pipe configuration. The ranges of superficial velocities were as follows: 0–24 m/s for air, and 0–0.5 m/s for both oil and water. Instead of keeping either liquid flow rate constant, Odozi kept the total liquid flow rate constant. Most of the experimental runs were within the slug flow regime. For the highest gas velocities ($U_G > 4$ m/s) full dispersion between oil and water within the slug (body + film) was observed. For that range of superficial gas velocities, the pressure always showed a peak (corresponding to the phase inversion point), at water-cut ratios that shifted towards higher values as the gas flow rate increased. This observation could be explained as follows: as the gas flow rate increases, the body of the slug would become more aerated, and the presence of gas bubbles would increase the water fraction required to invert the mixture. The peak of the pressure gradient could be predicted with a fairly good accuracy using the correlation of Beggs and Brill (1973) in conjunction with a non-linear model for the mixture viscosity (Odozi, 2000; Odozi et al., 1998) based on the Brinkman equation (1952).

Measurements that are apparently contradictory to the above trends can be found in the literature. For instance, Stapelberg and Mewes (1994), in contrast to the aforementioned investigators, did not notice any peak in the pressure drop in their experiments within the three-phase slug flow regime. Furthermore, these authors noticed that for low gas velocities ($U_G < 1$ m/s), the pressure gradient was bounded by the two-phase air–oil and air–water pressure gradient, whereas for higher values of gas velocities the three-phase pressure gradient was actually smaller than that of two-phase air–water slug flow.

Modelling work on three-phase slug flow is scarce when compared with that on two-phase flow. To the knowledge of the authors, only two references are available, and both concern the computer code PeTra (Larsen et al., 1997; Larsen and Hedne, 2001), which caters to four gas–liquid flow regimes (stratified, annular, slug, and dispersed), while assuming that the liquid phases always flow in a segregated state when in the stratified or slug flow regimes. The latest version of the method (Larsen and Hedne, 2001) accounts for liquid drop entrainment into the gas layer in three-phase stratified flow, and into the gas core in annular flow. The code is based on the transient one-dimensional three-fluid model (Barnea and Taitel, 1996) and solves five continuity equations (for gas, oil film, water film, oil droplets, and water droplets), three momentum equations (for oil film, water film, and for gas + oil droplets + water droplets), one mixture energy equation, and one pressure equation. Like in the OLGA (Bendiksen et al., 1991), and TACITE (Pauchon et al., 1994) two-phase codes a minimum slip criterion predicts the onset of slugging for the case of hydrodynamic slug formation. Terrain induced slugs are determined from the pipeline topography when large gradients of liquid hold-up are detected. Thus, the method, unlike the one presented here, is not of the "slug capturing" variety, in that the slugs are artificially introduced into the domain based on some local flow criteria. When slugs are predicted to form by either mechanism, a slug tracking option is then automatically activated (Zheng et al., 1994; Taitel and Barnea, 1998; Nydal and Banerjee, 1996), to follow the slugs using an adaptive moving grid in a Lagrangian frame. Like with other slug tracking techniques, closure relations (wall and interfacial friction factors, entrainment and deposition rates, and bubble nose velocity) are invoked. However, the method does not incorporate a model to account for all the possible liquid–liquid flow patterns that occur. The PeTra code has been tested (Larsen and Hedne, 2001) on a three-phase severe slugging case, with encouraging results.

The present work presents a mathematical model developed to simulate three-phase slug flow, and the calculations carried out to validate it. The present approach uses a two-fluid model to represent the gas and liquid mixture phases in conjunction with a drift–flux relation to account for the slip between the liquid phases. Thus, continuity and momentum equations are solved for the gas and the combined liquid phases. In order to close the model, a scalar transport equation for the conservation of mass of the water phase is formulated. Other closure models concern the liquid–liquid flow pattern (stratified or fully dispersed), the phase inversion point, the slip between the liquid phases and the friction factors. The numerical methodology applied is based on the slug capturing technique that was presented by Issa and Kempf (2003).

2. The model

2.1. The transport equations

The model is required to describe the flow of one gas and two liquid phases. The most obvious option here is to apply the three-fluid model set of equations (Barnea and Taitel, 1996). However, such a model introduces much additional complexity and demands much more computer resources compared to the two-fluid model for two-phase flow. A plausible alternative lies in the application of a drift–flux model (such as that used by Ishii, 1978) to the liquid motion, wherein the slip velocity is related to other quantities of the flow by an algebraic expression. Using a drift–

flux allows the reduction of the number of equations (and consequently of variables for which to solve). This is the approach adopted here, wherein the two liquids (say oil and water) are treated as a single liquid phase thereby reducing the number of transport equations from six to five. Although this reduction may not appear to be significant, in actual fact it greatly simplifies the numerical procedure needed to solve the equations, since:

(a) The reduced set has the same four main variables as the two-fluid model equations, namely, one phase fraction, the gas velocity, one liquid (mixture) velocity, and the interfacial pressure. The fifth variable (i.e. the phase fraction of one of the liquid phases) does not feature explicitly in the other transport equations, and can therefore be treated as an auxiliary quantity obtained separately from its own scalar transport equation.
(b) The mass fluxes which are required to satisfy overall continuity are only two (rather than three).
(c) The compatibility condition (phase fractions must sum to unity) involves only two-phase fractions; the third is obtained from an 'auxiliary' equation (being the continuity of one of the liquid phases).

As a consequence of the above factors, the new model is only marginally different from the two-fluid model that applies to two-phase flow, and can therefore (see Section 3 where the numerical procedure is outlined) be implemented without much effort in a numerical solution procedure based on the framework of the two-fluid model. Yet the model, as will be seen shortly, is able to handle three-phase slug flow remarkably well.

In the new approach, the information that determines the local liquid flow structure, such as the oil–water flow pattern, or the viscosity of the dispersion once the liquids become mixed, has to be fed into the equations by means of appropriate closure models. In the present approach, segregated (Fig. 1) and fully dispersed (Fig. 2) oil–water flows are catered for by the model. Clearly, these flow patterns represent an idealisation since, as was mentioned earlier, dispersions can still occur between stratified liquid layers thereby leading to more complex flow structures. However, it is felt that these additional complexities are of second order importance and that the essential features of the flow can be adequately represented by the present idealised model. However, an important phenomenon that plays a major role that must be catered for is phase inversion. To account for this flow feature, a correlation for the determination of the inversion point is introduced in order to identify which of the liquid phases is continuous and which is dispersed in the liquid mixture. A representative scheme of the possible combinations of liquid flow patterns is displayed in Fig. 3.

Fig. 1. Stratification of the liquid phases.

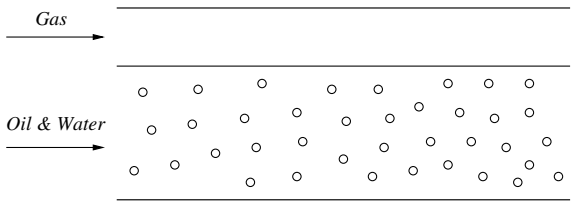

Fig. 2. Dispersion of the liquid phases.

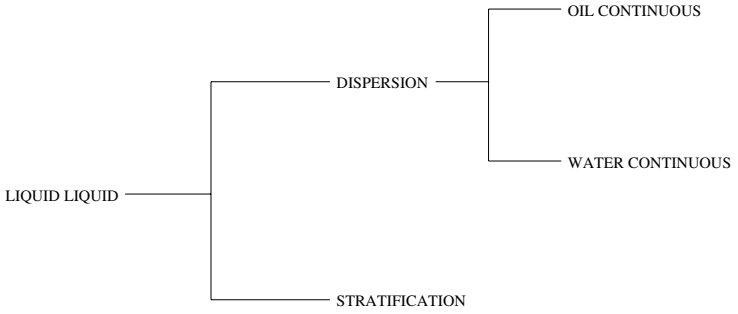

Fig. 3. Possible combinations of liquid–liquid flow patterns catered for by the present model.

The starting point in deriving the governing equations is the three-fluid model, in which transport equations are formulated for each phase (Barnea and Taitel, 1996). The continuity and momentum equations for the two liquids (say oil and water) are then combined together to obtain new equations in terms of liquid mixture quantities; details of this derivation are given in Bonizzi (2003) and are hence omitted here. The new mixture quantities are:

(i) the liquid phase hold-up α_M, given by the sum of the oil and water fractions ($\alpha_M = \alpha_O + \alpha_W$), related to the gas voidage α_G through the fundamental relation

$$\alpha_M + \alpha_G = 1, \tag{1}$$

(ii) the in situ water-cut c_W, defined by the ratio of water to total liquid hold-up ($c_W = \alpha_W/\alpha_M$)

(iii) the mixture density ρ_M, which is a linear function of oil and water densities given by:

$$\rho_M = (1 - c_W)\rho_O + c_W\rho_W; \tag{2}$$

(iv) the liquid centre of mass velocity u_M (Ishii, 1978), expressed as follows:

$$u_M = \frac{(1 - c_W)\rho_O u_O + c_W\rho_W u_W}{\rho_M}. \tag{3}$$

If the slip velocity between oil and water is defined as:

$$u_s = u_O - u_W, \tag{4}$$

then it is possible to derive expressions for the oil and water velocities from Eqs. (3) and (4) as:

$$u_{\mathrm{O}} = u_{\mathrm{M}} + \frac{c_{\mathrm{W}}\rho_{\mathrm{W}}u_{\mathrm{s}}}{\rho_{\mathrm{M}}}, \tag{5}$$

and

$$u_{\mathrm{W}} = u_{\mathrm{M}} - \frac{(1-c_{\mathrm{W}})\rho_{\mathrm{O}}u_{\mathrm{s}}}{\rho_{\mathrm{M}}}, \tag{6}$$

respectively. As shown later, the slip velocity is determined by a scalar equation that depends on the local liquid–liquid flow pattern.

In the present model, the gas is regarded as a compressible fluid obeying the ideal gas law, while both liquids are taken to be incompressible; the flow is treated as isothermal. The equations solved, for stratified unaerated slug three-phase flow, with no mass exchange between the phases, are as follows (Bonizzi, 2003):

- gas continuity equation:

$$\frac{\partial(\rho_{\mathrm{G}}\alpha_{\mathrm{G}})}{\partial t} + \frac{\partial(\rho_{\mathrm{G}}\alpha_{\mathrm{G}}u_{\mathrm{G}})}{\partial x} = 0, \tag{7}$$

- liquid phase (mixture) continuity equation:

$$\frac{\partial(\rho_{\mathrm{M}}\alpha_{\mathrm{M}})}{\partial t} + \frac{\partial(\rho_{\mathrm{M}}\alpha_{\mathrm{M}}u_{\mathrm{M}})}{\partial x} = 0, \tag{8}$$

- water-cut transport equation:

$$\frac{\partial(\rho_{\mathrm{W}}c_{\mathrm{W}}\alpha_{\mathrm{M}})}{\partial t} + \frac{\partial(\rho_{\mathrm{W}}c_{\mathrm{W}}\alpha_{\mathrm{M}}u_{\mathrm{W}})}{\partial x} = 0, \tag{9}$$

- gas momentum equation:

$$\frac{\partial(\rho_{\mathrm{G}}\alpha_{\mathrm{G}}u_{\mathrm{G}})}{\partial t} + \frac{\partial(\rho_{\mathrm{G}}\alpha_{\mathrm{G}}u_{\mathrm{G}}^2)}{\partial x} = -\alpha_{\mathrm{G}}\frac{\partial p}{\partial x} - \alpha_{\mathrm{G}}\rho_{\mathrm{G}}g\sin\beta - \frac{\tau_{\mathrm{GL}}S_{\mathrm{GL}}}{A} - \frac{\tau_{wG}S_{\mathrm{G}}}{A}, \tag{10}$$

- liquid phase (mixture) momentum equation:

$$\frac{\partial(\rho_{\mathrm{M}}\alpha_{\mathrm{M}}u_{\mathrm{M}})}{\partial t} + \frac{\partial(\rho_{\mathrm{M}}\alpha_{\mathrm{M}}u_{\mathrm{M}}^2)}{\partial x} = -\alpha_{\mathrm{M}}\frac{\partial p}{\partial x} - \alpha_{\mathrm{M}}\rho_{\mathrm{M}}g\frac{\partial h}{\partial x}\cos\beta - \alpha_{\mathrm{M}}\rho_{\mathrm{M}}g\sin\beta + \frac{\tau_{\mathrm{GL}}S_{\mathrm{GL}}}{A} - \frac{\sum_{K=1}^{N}\tau_{\mathrm{w}K}S_{\mathrm{K}}}{A} + \Omega + \Psi, \tag{11}$$

where the subscripts G, M, and W refer to the gas, mixture, and water phases respectively. The axial coordinate is x; the density is ρ; the phase fraction is α; the liquid-cut is c; the velocity is u; the interface (and gas) pressure is p; the liquid-mixture height is h; S_{L} and S_{G} are the liquid–wall, and gas–wall wetted perimeters respectively; S_{GL} represents the liquid–gas interfacial chord; τ is the shear stress; A is the pipe cross sectional area; the pipe inclination is β, and the acceleration due to gravity is g. The index N in the summation on the right hand side of Eq. (11) denotes the number of liquid phases in contact with the pipe walls; hence its value is 2 (i.e. oil and water) in case of stratified liquids, and 1 if the liquids are dispersed, since it is herein assumed that only the

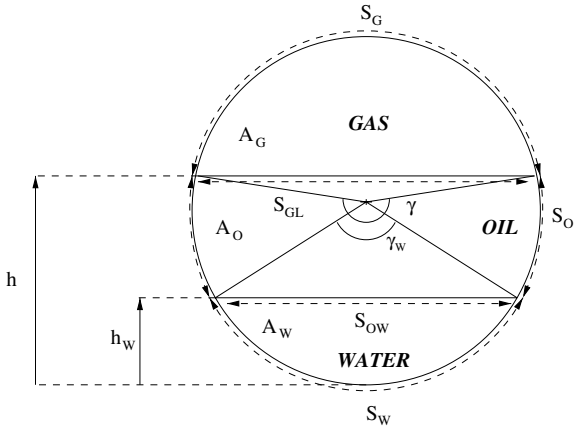

Fig. 4. Geometrical parameters for three-phase stratified flow with segregation of the liquid phases.

continuous liquid wets the pipe walls. The geometrical parameters are displayed in Fig. 4 which depicts the case of stratification among the three-phases.

The Ω and Ψ terms in Eq. (11) are given by the following relations:

$$\Omega = -\frac{\partial}{\partial x}\left[\frac{\alpha_M c_W (1-c_W)\rho_W \rho_O u_s^2}{\rho_M}\right], \tag{12}$$

and:

$$\Psi = \alpha_M(\rho_M - \rho_O)g\cos\beta\frac{\partial h}{\partial x} - \alpha_W(\rho_W - \rho_O)g\cos\beta\frac{\partial h_W}{\partial x}, \tag{13}$$

when the liquids flow in a segregated state; otherwise the latter is 0 if the liquids are fully dispersed. The derivatives of the liquid heights in Eq. (13) are related to the respective liquid fractions by:

$$\frac{\partial h}{\partial x} = \frac{\pi D}{4\sin(\gamma/2)}\frac{\partial \alpha_M}{\partial x} \tag{14}$$

and

$$\frac{\partial h_W}{\partial x} = \frac{\pi D}{4\sin(\gamma_W/2)}\frac{\partial \alpha_W}{\partial x} \tag{15}$$

here D is the pipe diameter and angles γ and γ_W denote the stratification angles for the total liquid and water layer respectively, as shown in Fig. 4.

An important feature of the model is the combination of the two liquid equations to yield mixture equations. This however, introduces a new variable, u_s, which is the slip velocity between the liquid phases; a closure relation is required to specify this velocity.

When the liquids are in the stratified state, the slip velocity is here calculated from the oil and water momentum equations assuming local equilibrium conditions (Ishii, 1978). Therefore, by neglecting derivatives with respect to time, static head and inertia terms in the original momentum equations, an expression for the slippage can be obtained as (Bonizzi, 2003):

$$u_s = \sqrt{\frac{2A}{f_{OW}\rho_O S_{OW}}\left|\frac{(1-c_W)\tau_{wW}S_W}{A} - \frac{c_W\tau_{wO}S_O}{A} + \frac{c_W\tau_{GO}S_{GO}}{A} + c_W\alpha_O(\rho_W-\rho_O)g\sin\beta\right|}, \quad (16)$$

where the wetted perimeters and interfacial widths are as shown in Fig. 4, and the oil–water interphase friction factor is denoted by f_{OW} (closure for the friction factors is the subject of Section 2.3).

When the liquid phases mix, thereby forming a dispersion, the mixture is treated as a homogeneous flow (i.e. with zero slippage, $u_s = 0$). This is a justifiable assumption provided that the two liquids have similar densities as is the case of water and oil considered here; otherwise, the slip velocity may not be negligible, in which case an appropriate closure model for it would be needed, but developing such a model is not a difficult task.

2.2. Characteristics analysis

The two-fluid model equations for stratified and slug flows (which contain the hydrostatic term, $\alpha\rho g\partial h/\partial x$) are conditionally hyperbolic and therefore can be well-posed as initial-value problem (see e.g. Banerjee and Chan, 1980; Issa and Kempf, 2003). The task here is to investigate the nature of the new proposed model, and to establish that the system is still conditionally well-posed. In what follows, a study of the characteristics for the proposed set of equations is carried out, and this will show that for the cases considered (in the validation exercise presented later), real characteristics exist.

The set of Eqs. (7)–(11) represents a system of first order partial differential equations that can be written in a compact form as:

$$A\frac{\partial \Phi}{\partial t} + B\frac{\partial \Phi}{\partial x} = C, \quad (17)$$

where A and B are coefficient matrices (of dimension 5 by 5 in the present case), Φ is the solution vector here corresponding to

$$\Phi = [\alpha_G, c_W, u_G, u_M, p]^T, \quad (18)$$

and C is a vector containing all the algebraic terms. The initial value problem under consideration is to find a solution of system (17) in some region:

$$a \leqslant x \leqslant b, \quad t \geqslant 0, \quad (19)$$

subject to the initial condition:

$$\Phi(t=0,x) = G(x), \quad (20)$$

and values of Φ or its derivatives defined on the boundaries $x = a$ and $x = b$. The system (17) is defined to be well-posed (or hyperbolic) when the equations with appropriate boundary conditions and initial values admit a unique solution and this solution depends continuously on the initial data and boundary conditions. The mathematical character of a set of partial differential equations is provided by the solution of the *eigenvalue system* (Hirsch, 1988):

$$\det[B - \lambda A] = 0. \quad (21)$$

A necessary condition for the system to be well-posed, is that the roots (that physically represent the characteristics of the system) of Eq. (21) are all real and distinct. These characteristics represent the velocities at which the information travels through the domain.

Although gas compressibility effects are taken into account in the present model, the analysis of the compressible form of the model equations is too complex to present here. In any event, such analysis is deemed unnecessary, since the non-hyperbolicity problem arises equally with incompressible fluids. Hence, in order to simplify the analysis, the gas phase is here treated as incompressible (but only for the purpose of the characteristics analysis). Furthermore, the analysis is carried out for a horizontal pipe ($\beta = 0$).

When all differential terms in Eqs. (7)–(11) are expressed as function of the unknowns of the solution vector (Eq. (18)), the coefficient matrices A and B become respectively:

$$A = \begin{bmatrix} 1 & 0 & 0 & 0 & 0 \\ -\rho_M & \alpha_M(\rho_W - \rho_O) & 0 & 0 & 0 \\ -c_W & \alpha_M & 0 & 0 & 0 \\ u_G\rho_G & 0 & \alpha_G\rho_G & 0 & 0 \\ -u_M\rho_M & u_M\alpha_M(\rho_W - \rho_O) & 0 & u_M\rho_M & 0 \end{bmatrix}, \tag{22}$$

and

$$B = \begin{bmatrix} u_G & 0 & \alpha_G & 0 & 0 \\ -\rho_M u_M & \alpha_M u_M(\rho_W - \rho_O) & 0 & \alpha_M\rho_M & 0 \\ -c_W u_M + \frac{c_W(1-c_W)\rho_O u_s}{\rho_M} & \alpha_M u_M - \frac{\alpha_M\rho_O u_s(\rho_O(1-c_W)^2 - \rho_W c_W^2)}{\rho_M^2} & 0 & c_W\alpha_M & 0 \\ \rho_G u_G^2 & 0 & 2\alpha_G\rho_G u_G & 0 & \alpha_G \\ \Theta & Z & 0 & 2\alpha_M\rho_M u_M & \alpha_M \end{bmatrix}, \tag{23}$$

where the first two coefficients in the last row of the B matrix are given by

$$\Theta = -\rho_M u_M^2 - \alpha_M\rho_M g\overline{D}_L + c_W\alpha_M(\rho_W - \rho_O)g\overline{D}_L - c_W^2\alpha_M(\rho_W - \rho_O)g\overline{D}_W - \frac{(c_W - c_W^2)\rho_O\rho_W u_s^2}{\rho_M}, \tag{24}$$

and

$$Z = \alpha_M(\rho_W - \rho_O)u_M^2 + c_W\alpha_M^2(\rho_W - \rho_O)g\overline{D}_W + \frac{\alpha_M\rho_W\rho_O u_s^2(\rho_O(1 - c_W)^2 - \rho_W c_W^2)}{\rho_M^2}, \tag{25}$$

respectively, where $\overline{D}_L$ and $\overline{D}_W$ are defined from Eqs. (14) and (15) as $\pi D/(4\sin(\gamma/2))$ and $\pi D/(4\sin(\gamma_W/2))$ respectively. The characteristics equation can then be formulated by inserting the matrix expressions given by (22)–(25) into Eq. (21); the resulting cubic equation in the eigenvalue λ is too long to present here and is omitted for brevity. Moreover, the analytic solution to that equation is quite complicated and tedious; instead, the roots are computed here numerically to illustrate the existence of real characteristics. Such numerical evaluation needs as input, values of the gas and liquid phase fractions as well of the velocities. Two such calculations are presented here for typical values of flow variables arising in actual slug flow cases investigated

experimentally and used in the validation study presented in Section 4. The cases relate to three-phase gas–oil–water slug flow, where the air and total liquid superficial velocities are 4.0 and 0.5 m/s respectively. Figs. 5 and 6 show the computed characteristics of the system, plotted versus the whole spectrum of water-cuts, for two different values of the gas void fractions (0.1 and 0.7 respectively). These values pertain to regions in the flow where a slug is about to form ($\alpha_g = 0.1$) and where a thin liquid film exists ($\alpha_g = 0.7$). As can be seen from the diagrams, the three characteristic velocities λ_1, λ_2, λ_3 are all real and distinct in both cases, thus verifying that the governing equations (6)–(10) are hyperbolic for the given conditions. This has also been verified for numerous other flow conditions with different values of α_g. It can also be observed that the values of the eigenvalues are all positive hence implying that the characteristics run in the direction of the flow.

When gas compressibility is accounted for, two more eigenvalues (i.e. characteristics), λ_4 and λ_5 can be found (Bonizzi, 2003). These are related to compressibility waves and are given by:

$$\lambda_{4,5} \approx \pm c, \tag{26}$$

where c is the speed of sound.

It is clear that for some flow conditions, with gas compressibility accounted for, the equation system is well posed with five characteristics present, four running in the direction of the flow, and the fifth in the opposite direction. This therefore dictates the number of boundary conditions to be imposed: four quantities must be specified at inlet and one at outlet.

It should be remarked, that the equation system is only conditionally well-posed and some flow conditions can result in an ill-posed system, in which case a unique numerical solution is unobtainable as demonstrated in the case of two-phase flow by Issa and Kempf (2003). Such cases are avoided in the present work.

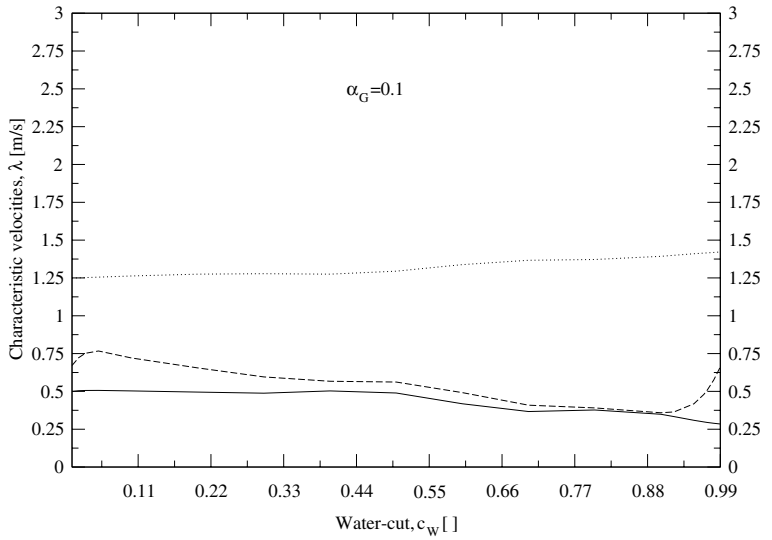

Fig. 5. Characteristic velocities calculated from hyperbolicity study of the governing equations for a gas–oil–water stratified flow with a gas voidage of 0.1. Gas and total liquid superficial velocities of 4.0 and 0.5 m/s respectively.

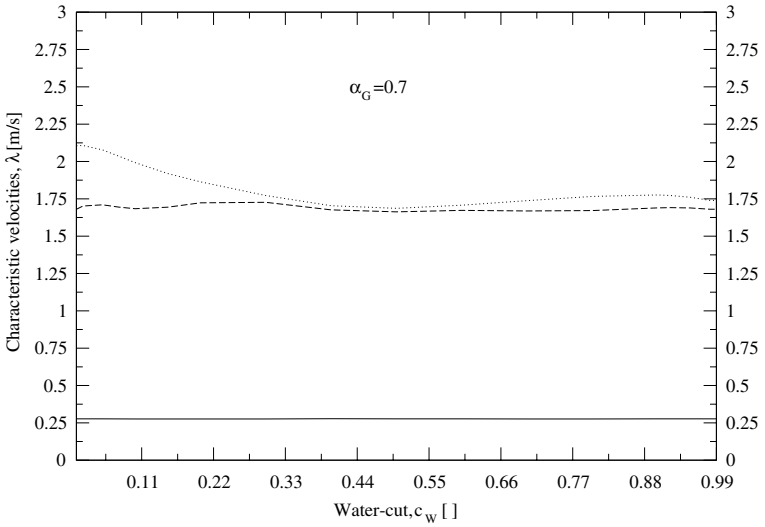

Fig. 6. Characteristic velocities calculated from hyperbolicity study of the governing equations for a gas–oil–water stratified flow with a gas voidage of 0.7. Gas and total liquid superficial velocities of 4.0 and 0.5 m/s respectively.

2.3. Model for determination of phase inversion and liquid–liquid flow pattern

Most of the available literature on phase inversion, concerns two-phase liquid–liquid flow (Arirachakaran et al., 1989; Nädler and Mewes, 1995; Decarre and Fabre, 1997; Brauner and Ullmann, 2002). To the knowledge of the present authors, no theoretical investigation into this phenomenon has been made in three-phase gas–liquid–liquid systems. All that exists in the literature are different correlations for the calculation of the phase inversion point.

Phase inversion in three-phase gas–oil–water flows was studied experimentally by several authors, such as Malinowsky (1975), Pan (1996), and Odozi (2000). In general these investigators found that the phase inversion is a strong function not only of the total liquid mixture velocity, but also of the gas superficial velocity. Utvik et al. (1998) reported a shift in the phase inversion point from 40–50% at low gas fractions, to up to 95% for very high gas fractions. Valle (1998) suggested that gas bubbles would inhibit the coalescence of oil drops at very high gas fractions (where the gas aeration is enhanced), therefore increasing the value of water fraction that would lead to inversion of the liquid/liquid mixture. This was also found to be true by Odozi (2000), who curve-fitted his experimental data with the following expression:

$$\Gamma_W^{inv} = 0.3372\ U_G^{0.2219}, \tag{27}$$

where Γ_W^{inv} represents the water fraction at the inversion point ($\Gamma_W = U_W/(U_O + U_W)$). The above equation is a crude fit to the data, and is given as function of the gas superficial velocity only. It is therefore of limited generality since it is not non-dimensional and does not involve any surface chemistry or physical property of the liquid phases.

The most comprehensive model for phase inversion that caters for the important physical phenomena appears to be that of Decarre and Fabre (1997). This model, as it will be seen shortly,

accounts for both turbulent and laminar dispersions; the capability of predicting the occurrence of the latter is extremely important, especially when highly viscous oils are used. Although the model was developed for two-phase flow, it is herein extended to three-phase flows assuming that the oil and water locally flow in an equivalent pipe with a diameter corresponding to that hydraulic $D_M = 4A_M/S_M$.

The Decarre & Fabre model is based on principles of thermodynamics for the minimisation of the total system energy, assuming local homogeneous flow between the phases. Hence, from Eqs. (5) and (6) one can deduce that the liquid dispersion flows at the velocity of the centre of mass u_M. Now, the Reynolds numbers of the liquids are defined as:

$$Re_K = \frac{\rho_K u_M D_M}{\mu_K}. \tag{28}$$

with K denoting either oil or water.

There exist three possible situations when phase inversion occurs: (i) flow conditions in which the flow regime remains laminar ($Re_K \leqslant 2100$) regardless of which phase is continuous and which is dispersed, (ii) flow conditions in which the flow regime remains turbulent ($Re_K > 2100$), or (iii) flow conditions in which there is a mixed laminar/turbulent flow regime (for instance $Re_O \leqslant 2100$ and $Re_W > 2100$). For each of the three possible conditions, Decarre & Fabre derived related equations to determine the phase inversion. These are:

$$\Gamma_W^{inv} = 1 - \left\{ 1 + \left(\frac{\mu_W}{\mu_O} \right)^{2/3} \right\}^{-1}, \tag{29}$$

for a flow regime remaining laminar ($Re_K \leqslant 2100$) when inversion occurs,

$$\Gamma_W^{inv} = 1 - \left\{ 1 + \left(\frac{\mu_W}{\mu_O} \right)^{1/14} \left(\frac{\rho_W}{\rho_O} \right)^{5/14} \right\}^{-1}, \tag{30}$$

for a flow regime remaining turbulent ($Re_K > 2100$) when inversion occurs, and

$$\frac{(\Gamma_W^{inv})^{7/5}}{1 - \Gamma_W^{inv}} = \frac{0.145}{1.15 \times 2^{3/5}} (\sigma_{OW} f_{wW})^{2/5} (D_M \rho_W)^{3/5} \frac{u_M^{0.2}}{\mu_O^{5/6} \mu_W^{1/6}}, \tag{31}$$

for a flow regime being laminar when the oil is the continuous phase, and turbulent when the water is the continuous phase. In the above equations, σ_{OW} represents the oil–water surface tension, and f_{wW} the water-wall friction factor.

In order to determine locally (i.e. inside each control volume of the computational mesh) which phase is continuous and which is dispersed when the liquids are mixed, the following inequality has to be continually checked:

$$c_W \geqslant \Gamma_W^{inv}. \tag{32}$$

If relation (32) is satisfied, then water is considered to be the continuous phase; otherwise it is the oil.

In order to establish whether the oil–water flow is within the dispersed flow regime (as opposed to stratified) the maximum droplet size (d_{max}) that can generate under the specific flow conditions

and physical properties of the liquids needs to be determined first. In fully turbulent conditions, the droplet size that originates can be obtained (according to Hinze, 1955) from a critical Weber number $We_{\mathrm{crit}} = \tau d_{\max}/\sigma$ where τ represents the shear force acting on the droplet and σ is the liquid/liquid surface tension. Here the value of the critical Weber number of 1.17 as recommended by Brauner (2001) is used. In the case when the continuous phase flows in a laminar state the value of $d_{\max}$ may be found following the recommendation of Decarre & Fabre who used the solution of the Stokes equations by Hinch and Acrivos (1979) for droplet break-up in a two-dimensional straining motion; that solution is given by the left hand side of Eq. (34) below. Next, it is necessary to determine values of the critical droplet size (d_{crit}) above which liquid–liquid dispersions cannot exist. This critical droplet diameter is usually arrived at by considering agglomeration effects that tend to lead to droplet coalescence, as well as of migration of droplets to the upper part of the wall (phenomenon termed as creaming) due to buoyancy (Barnea, 1986). The approach proposed by Brauner and Moalem Maron (1992) and by Brauner (2001), and adopted here, stipulates that for the transition from stratified to fully dispersed regimes to occur, $d_{\max}$ must be smaller or equal to d_{crit}. This therefore leads to the following criteria:

$$\frac{1.15D_{\mathrm{M}}}{2^{2/5}}\left(\frac{\rho_{\mathrm{c}}D_{\mathrm{M}}u_{\mathrm{M}}^2}{\sigma_{\mathrm{OW}}}\right)^{-0.6}\left(\frac{f_{\mathrm{c}}}{(1-c_{\mathrm{d}})}\right)^{-0.4} \leqslant \mathrm{Min}\left\{\sqrt{\left(\frac{6.0\sigma_{\mathrm{OW}}}{|\rho_{\mathrm{W}}-\rho_{\mathrm{O}}|g\cos\beta}\right)}, \frac{3}{8}\frac{\rho_{\mathrm{c}}}{|\rho_{\mathrm{W}}-\rho_{\mathrm{O}}|}\frac{f_{\mathrm{c}}u_{\mathrm{M}}^2}{g\cos\beta}\right\}, \tag{33}$$

when the continuous phase flow is turbulent; otherwise:

$$\frac{0.145}{2}D_{\mathrm{M}}\frac{\sigma_{\mathrm{OW}}}{\mu_{\mathrm{c}}u_{\mathrm{M}}}\left(\frac{\mu_{\mathrm{d}}}{\mu_{\mathrm{c}}}\right)^{-\frac{1}{6}} \leqslant \sqrt{\left(\frac{6.0\sigma_{\mathrm{OW}}}{|\rho_{\mathrm{W}}-\rho_{\mathrm{O}}|g\cos\beta}\right)}, \tag{34}$$

if the dispersion is laminar. In Eqs. (33) and (34) subscripts c and d denote continuous and dispersed phase respectively. If the values of the liquid densities approach each other, the critical drop sizes on the right hand sides of Eqs. (33) and (34) would tend to infinity, and therefore would lose its physical meaning. Under these circumstances, Brauner (2001) suggested that for Eötvös numbers defined as:

$$Eo = \frac{|\rho_{\mathrm{W}}-\rho_{\mathrm{O}}|gD_{\mathrm{M}}^2}{8\sigma_{\mathrm{OW}}} \tag{35}$$

smaller than 0.2, the critical drop size should be scaled with the pipe diameter D_{M}, and recommended to take $d_{\mathrm{crit}} \approx 0.5D_{\mathrm{M}}$.

2.4. Friction factors

In the case of liquid stratification in three-phase flow, five shear stresses must be defined. These are: the wall shear stresses for water τ_{wW}, oil τ_{wO}, and gas τ_{wG}, as well as the interfacial shear stresses between the gas and the liquid phase τ_{GL}, and that between the oil and water τ_{OW}. These are defined as follows:

$$\tau_{\mathrm{wW}} = f_{\mathrm{wW}}\frac{\rho_{\mathrm{W}}|u_{\mathrm{W}}|u_{\mathrm{W}}}{2}, \tag{36}$$

$$\tau_{wO} = f_{wO}\frac{\rho_O|u_O|u_O}{2}, \tag{37}$$

$$\tau_{wG} = f_{wG}\frac{\rho_G|u_G|u_G}{2}, \tag{38}$$

$$\tau_{GL} = f_{GL}\frac{\rho_G|u_G - u_K|(u_G - u_K)}{2}, \tag{39}$$

and

$$\tau_{OW} = f_{OW}\frac{\rho_O|u_O - u_W|(u_O - u_W)}{2}, \tag{40}$$

respectively. The subscript K in Eq. (39) denotes the liquid phase in contact with the gas (i.e. oil if the liquids flow in a stratified state or if the dispersion is oil-based, or water if the dispersion is water-based). The wall friction factors are calculated using the same correlations applied to two-phase slug flow (Issa and Kempf, 2003). In particular, the Hand formula (1991) is used for the liquid wall friction factor:

$$f_wK = \frac{24}{Re_K}, \tag{41}$$

for laminar flow ($Re_K \leqslant 2100$), and

$$f_{wK} = 0.0262(\alpha_K Re_K)^{-0.139}, \tag{42}$$

for turbulent flow ($Re_K > 2100$), where the subscript K stands for either the oil or water phase. The liquid Reynolds number is defined as follows:

$$Re_K = \frac{\rho_K u_K D_K}{\mu_K}, \tag{43}$$

where the liquid phase hydraulic diameter is expressed as:

$$D_K = \frac{4A_K}{S_K}. \tag{44}$$

The gas wall friction factor is given by the following equation:

$$f_{wG} = C_G Re_G^{-n_G}, \tag{45}$$

where the gas hydraulic diameter is defined as:

$$D_G = \frac{4A_G}{S_G + S_{GL}}. \tag{46}$$

The coefficients C_G and n_G in Eq. (45) take the values of 0.045 and 0.25 if the gas flows in a turbulent state, or 16 and 1 if laminar. The oil–water interfacial friction factor is chosen to be a fixed value, following the recommendations of Taitel et al. (1995) and Khor et al. (1997):

$$f_{OW} = 0.014. \tag{47}$$

If the oil and water disperse, the oil–water shear stress becomes redundant (as it is subsumed into the drift–flux relation used to specify the slip velocity). The liquid–wall friction factor is still

calculated from Eqs. (41) and (42) but using the properties of the liquid mixture. Hence, the liquid Reynolds number is calculated as follows:

$$Re_{\mathrm{M}} = \frac{\rho_{\mathrm{M}} u_{\mathrm{M}} D_{\mathrm{M}}}{\mu_{\mathrm{M}}}, \tag{48}$$

where the mixture viscosity is calculated using the Brinkman law (1952):

$$\mu_{\mathrm{M}} = \frac{\mu_{\mathrm{c}}}{(1 - c_{\mathrm{d}})^{2.5}}. \tag{49}$$

The liquid–wall shear stress is given by the following expression:

$$\tau_{\mathrm{wL}} = f_{\mathrm{wL}} \frac{\rho_{\mathrm{M}} |u_{\mathrm{M}}| u_{\mathrm{M}}}{2}. \tag{50}$$

The gas–liquid interfacial friction factor is expressed as:

$$f_{\mathrm{GL}} = C_{\mathrm{i}} Re_{\mathrm{i}}^{-n_{\mathrm{i}}}, \tag{51}$$

where the inter-phase Reynolds number is given by:

$$Re_{\mathrm{i}} = \frac{\rho_{\mathrm{G}} |u_{\mathrm{G}} - u_{\mathrm{K}}| D_{\mathrm{G}}}{\mu_{\mathrm{G}}}. \tag{52}$$

The coefficients C_{i} and n_{i} are calculated as in Eq. (45).

3. Numerical implementation

The equations solved by the model are (7)–(11), with a solution vector consisting of the following primitive variables: gas void fraction, water-cut, gas and liquid velocities, and interfacial pressure. There are strong similarities between the new three-phase slug flow algorithm and the existing technique for two-phase flow of Issa and Kempf (2003), the main difference being that the liquid phase is now composed of two liquid components (i.e. oil and water). There is now one more transport equation to be solved for the water fraction in the liquid mixture (Eq. (9)). Therefore, the three-phase algorithm could easily be implemented in the framework of the existing methodology, and the main features of the code remain practically unaltered. The equations are discretised using the finite volume formulation, with Euler-implicit discretisation in time, and first order upwind in space. The grid arrangement is staggered (i.e. the scalar properties are stored at the centres of the control volumes, and the velocities at the cells faces) as described by Issa and Kempf (2003). Fig. 7 shows the staggered grid arrangement for the one-dimensional domain, and depicts control volumes for the velocities and scalar-variables. In the figure, symbols e and w denote the boundaries of the cells that are centred on node p. The finite volume formulation of the continuity equation, integrated between the times t^o and $t^n = t^o + \Delta t$, is given, for either gas or liquid, by:

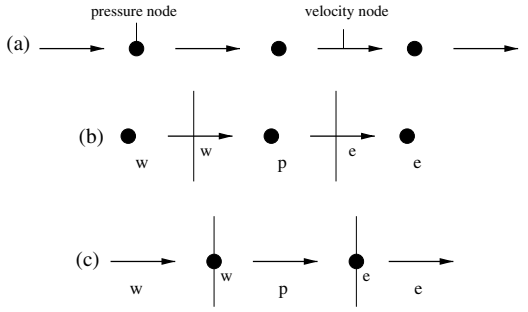

Fig. 7. Staggered grid arrangement. (a) Staggered mesh, (b) Scalar control volume, (c) Velocity control volume.

$$\left(\frac{\Delta x}{\Delta t}\rho_p^n + \max[\rho_w^n u_w^n, 0] + \max[-\rho_e^n u_e^n, 0] + (\rho_e^n u_e^n - \rho_w^n u_w^n)\right)\alpha_p^n = \max[\rho_w^n u_w^n, 0]\alpha_w^n + \max[-\rho_e^n u_e^n, 0]\alpha_e^n + \frac{\Delta x}{\Delta t}\rho_p^o \alpha_p^o, \tag{53}$$

that can be written in a more compact form as:

$$a_p \alpha_p^n = a_w^n \alpha_w^n + a_e^n \alpha_e^n + S_\alpha, \tag{54}$$

where a_e, a_w and a_p are finite difference coefficients representing the convective fluxes and S_α containing the rest of the terms. The discretised momentum equation is as follows:

$$\left(\frac{\Delta x}{\Delta t}\rho_p^n \alpha_p^n + \max[-\rho_e^n \alpha_e^n u_e^n, 0] + \max[\rho_w^n \alpha_w^n u_w^n, 0] + (\rho_e^n \alpha_e^n u_e^n - \rho_w^n \alpha_w^n u_w^n)\right)u_p^n = \max[\rho_w^n \alpha_w^n u_w^n, 0]u_w^n + \max[-\rho_e^n \alpha_e^n u_e^n, 0]u_e^n - \alpha_p^n(p_e^n - p_w^n) + \frac{\Delta x}{\Delta t}\rho_p^o \alpha_p^o u_p^o + S_u, \tag{55}$$

where S_u accounts for the whole of the source terms in Eqs. (10) and (11). Eq. (55) can be written in a more compact form using the operator H that stands for the finite-volume representation of the spatial convective fluxes, as:

$$\frac{\Delta x}{\Delta t}\left(\rho_p^n \alpha_p^n u_p^n - \rho_p^o \alpha_p^o u_p^o\right) = H_u(u_p^n) - \alpha_p^n(p_e^n - p_w^n) + S_u. \tag{56}$$

An overall continuity equation can now be obtained by combining the two continuity equations for the gas and liquid phases (7) and (8), each weighted by its related density, to give:

$$\frac{\Delta x}{\Delta t}\left(\frac{1}{\rho_{\mathrm{M}}^{ref}}(\alpha_{\mathrm{M},p}^n \rho_{\mathrm{M},p}^n - \alpha_{\mathrm{M},p}^o \rho_{\mathrm{M},p}^o) + \frac{1}{\rho_{\mathrm{G}}^{\mathrm{ref}}}(\alpha_{\mathrm{G},p}^n \rho_{\mathrm{G},p}^n - \alpha_{\mathrm{G},p}^o \rho_{\mathrm{G},p}^o)\right) + \frac{1}{\rho_{\mathrm{M}}^{ref}}(\alpha_{\mathrm{M},e}^n \rho_{\mathrm{M},e}^n u_{\mathrm{M},e}^n - \alpha_{\mathrm{M},w}^n \rho_{\mathrm{M},w}^n u_{\mathrm{M},w}^n) + \frac{1}{\rho_{\mathrm{G}}^{\mathrm{ref}}}(\alpha_{\mathrm{G},e}^n \rho_{\mathrm{G},e}^n u_{\mathrm{G},e}^n - \alpha_{\mathrm{G},w}^n \rho_{\mathrm{G},w}^n u_{\mathrm{G},w}^n). \tag{57}$$

If the velocities as expressed in Eq. (56), are now substituted into the above overall continuity equation (for details see Bonizzi, 2003), an equation for the pressure is then obtained in the form:

$$a_p^n p_p^n = a_w^n p_w^n + a_e^n p_e^n + S_p. \tag{58}$$

It is clear from Eq. (57) that the mass fluxes that guarantee satisfaction of the overall continuity are only those for the gas and composite liquid phases (i.e. $\alpha_G\rho_G u_G$ and $\alpha_M\rho_M u_M$), and this is the very feature that makes the new model for three-phase flow practically equivalent (from a computational point of view) to that for two-fluid flow as described by Issa and Kempf (2003). This similarity consequently leads to a relative easy implementation of the numerical procedure into an already existing one-dimensional code based on the two-fluid model equations (such as the TRIOMPH code used by Issa and Kempf, 2003).

A sequential iterative method is used to solve the system of discretised equations at each time step. The equations solved in the sequence are as follows:

- The liquid component momentum equation (11) which gives the liquid velocity;
- The gas momentum equation (10) yielding the gas velocity;
- The pressure equation (57) for the pressure which is then used to update the liquid and gas velocities to satisfy overall continuity;
- The gas continuity equation (7) which yields the gas phase fraction;
- The water-cut equation (9) that gives the water phase fraction.

Each of the sets of Eqs. (7), (9)–(11), (57) constitutes a tridiagonal matrix system which can be solved directly using coefficients based on old iteration values. The iteration loop is executed until the residuals in each equation become smaller than a fixed tolerance. Once convergence is achieved for the given step, a new time increment is calculated based on the following dimensionless number:

$$\frac{u^n_{G,\max}\Delta t}{\Delta x} = C, \tag{59}$$

where the quantity C in Eq. (59) is typically set at 0.5.

The boundary conditions imposed must reflect both the physics and the mathematical character of the governing equations (see Section 2.2). Here, five quantities (corresponding to the five characteristics of the equations) must be specified, four at inlet and one at outlet (dictated by the directions of the characteristics). At the inlet of the pipe the total liquid hold-up, and the superficial velocities of the gas, oil, and water are specified and assumed to remain steady at those values. At the outlet, the pressure is prescribed. The initial conditions correspond to stratified flow with uniform velocity, phase fractions, and pressure fields.

While the information about the liquid–liquid flow pattern is determined from closure models, that relating to the gas–liquid pattern is predicted automatically from the numerical solution of the conservation equations. Liquid slugs still generate automatically and are captured in the same way as in two-phase flow using the "slug capturing" methodology (Issa and Woodburn, 1998; and Issa and Kempf, 2003). The method, allows liquid slugs to be captured as a mechanistic and automatic outcome of the growth of hydrodynamic instabilities in an Eulerian frame.

In order to capture the natural growth of disturbances at the gas–liquid interface, the numerical resolution must be high. In order to achieve such accuracy with the currently used first order spatial and temporal discretisation schemes, very fine computational grids were utilised (typically $\Delta x/D \approx 0.4$ was found to be sufficient). Systematic checks were carried to verify that all the results are independent of the grid. Fig. 8 for instance shows the results of a grid dependency study,

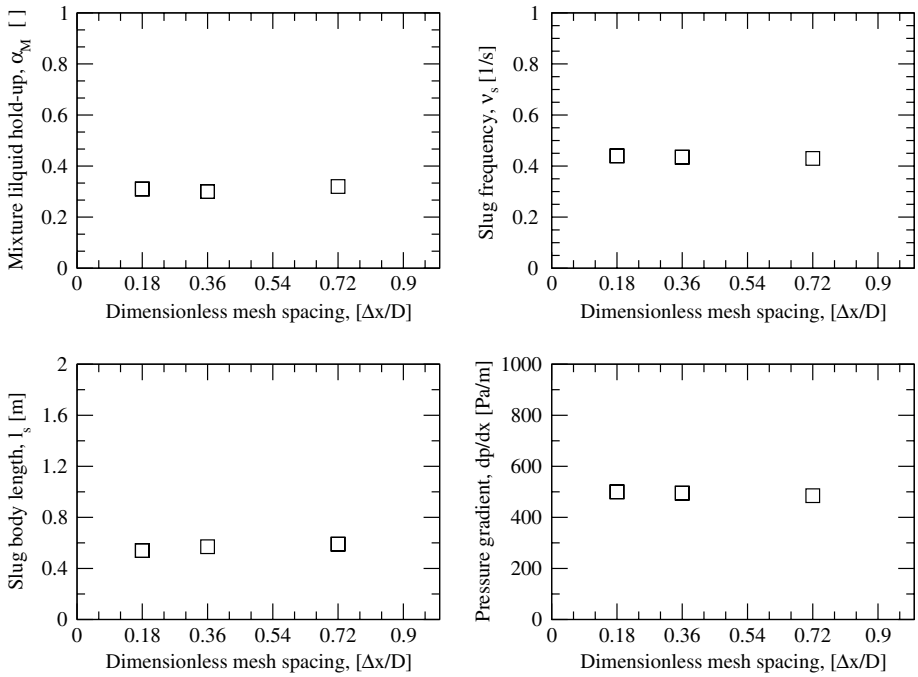

Fig. 8. Predicted slug characteristics versus dimensionless mesh spacing for a three-phase slug flow test case.

related to one of the calculations, where the predicted (statistically steady) total liquid hold-up, slug frequency, slug body length, and pressure gradient are plotted against the dimensionless mesh size. From the figure, it is apparent that the numerical results are independent of the mesh spacing, indicating convergence to a single specific solution (and thereby also verifying the well-posed nature of the equations for those flow conditions).

4. Results and discussion

The calculations using the model are validated against two sets of experimental measurements. The first experiment was performed by Odozi (2000) who used water at atmospheric condition, and oil of density 865 kg/m^3, and dynamic viscosity 48.0×10^{-3} Pa s. The pipe was horizontal, 38.0 m long, and with an internal diameter of $D = 0.078$ m. The superficial velocities of the gas and liquid were 4.0 and 0.5 m/s respectively; Odozi kept constant the total liquid superficial velocity, and examined the flow behaviour for the whole spectrum of inlet water-cuts, ranging from 0 (limit corresponding to two-phase air–oil flow), to 1 (that corresponds to two-phase air–water flow). It should be remarked that the experimental measurements are subject to errors estimated to be around ±5% for the phase hold-ups, and around ±0.5% for the pressure gradient (Hale and Hewitt, 2001). In the simulations, the oil–water surface tension was taken as $\sigma_{OW} = 0.03$ N/m and from the given values of liquid viscosities, the effective viscosity of the liquid mixture was calculated using the Brinkman law (Eq. (36)). Fig. 9 shows how the effective viscosity varies with

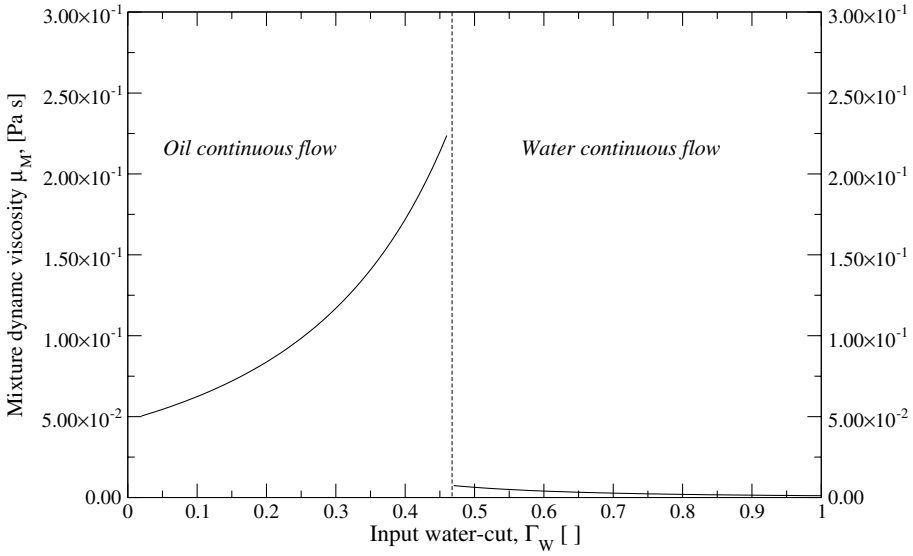

Fig. 9. Effective viscosity of oil–water mixture when Brinkman law is applied (1952).

water-cut; it should be noted that the figure incorporates an assumed inversion point at $\Gamma_W^{inv} = 0.47$. (this value being estimated from the data). The gas used is air with standard density of 1.2 kg/m^3, and viscosity of 1.77×10^{-5} Pa s. Regardless of the volumetric rates of the two liquids, the observed flow pattern was always slug flow.

By application of Eq. (30) of the Decarre & Fabre model, phase inversion was predicted to occur at a water-cut of 0.44. This value reflects, with good accuracy, the inversion region experimentally found by Odozi to occur at water-cuts between 0.45 and 0.48.

The kind of information that is typically extracted from a simulation is shown in Fig. 10, where the phase fractions along the pipe are plotted. The predictions are for a case where the inlet water-cut is 0.4, which is close to the phase inversion point ($\Gamma_W = 0.44$) as predicted by Eq. (30). In the figure, each phase is represented by a different shade: gas is clear, oil is light shaded and water is

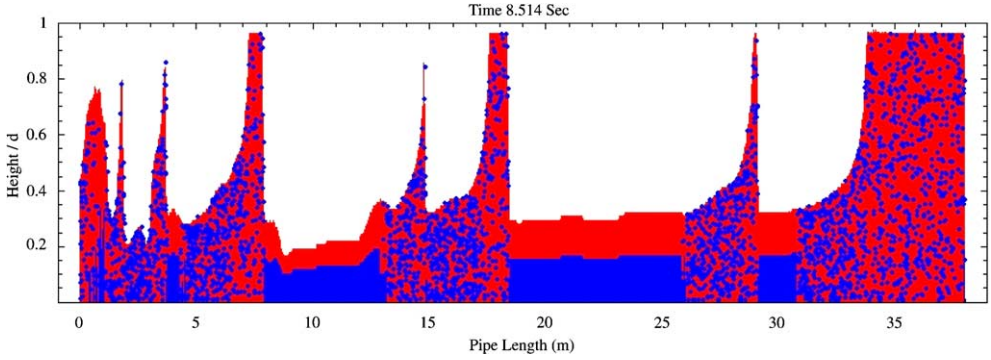

Fig. 10. Snapshot of three-phase slug flow animation. Gas in white, oil in light shade (red) and water in dark shade (blue).

dark. The predicted flow field is at an instant when slugs have already formed in the pipe, thereby illustrating the slug capturing capability. The liquid–liquid flow pattern that generates locally in the pipe is depicted either as dispersed (with liquid droplets represented by dots) or stratified (indicated by separate liquid layers). It is interesting to observe that the liquids mix in the body of the slugs, and in parts of the liquid films as well and become stratified in the film. After the simulation is run for sufficiently long time to allow all slug characteristics to reach their statistically "steady" values, the slug size distribution can be determined in the manner described by Issa and Kempf (2003). Histograms of slug length distributions such as that shown in Fig. 11, which pertains to the flow conditions mentioned above, can whence be constructed.

Fig. 12 displays the comparisons between experiments and predictions for the three-phase pressure gradient. Like all other slug characteristics that are analysed in the present work, the values are time averaged and calculated at a location close to the pipe exit for different values of the inlet water-cut. The experimental data show a sharp increase in the pressure gradient as the inlet water-cut approaches the inversion point. At a value of $\Gamma_W = 0.41$, the pressure gradient is about twice as great as that for two-phase air–oil slug flow. As the inversion point is crossed, there is an abrupt drop in the value corresponding to the sudden drop in mixture viscosity seen in Fig. 9. As the water volumetric flow rate increases, the pressure gradient tends towards the value for air–water slug flow, which is lower than the value for air–oil slug flow. The dashed line in Fig. 12 represents the inversion point according to Eq. (30) of the Decarre & Fabre model. It is evident that the predictions of the model (displayed by the diamond shaped symbols in the figure) reproduce fairly well the experimental trend: in the oil continuous region, the position of the peak is around a water-cut value of 0.41, close to the phase inversion point, as in the experiments. The numerical results consistently under-predict the experimental measurements even at the extremes of two-phase flow (water-cuts of 0 and 1), with a maximum discrepancy of 35% for an inlet

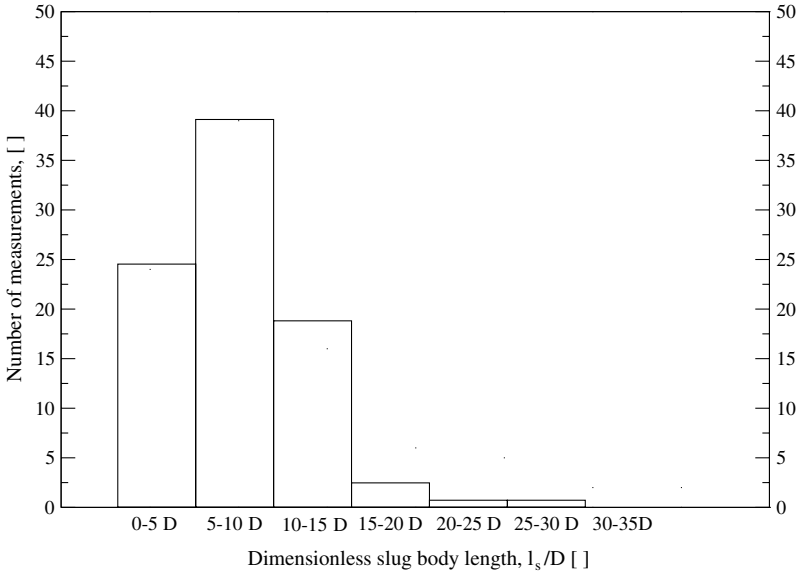

Fig. 11. Slug length distribution for a typical run with input water-cut of 0.4.

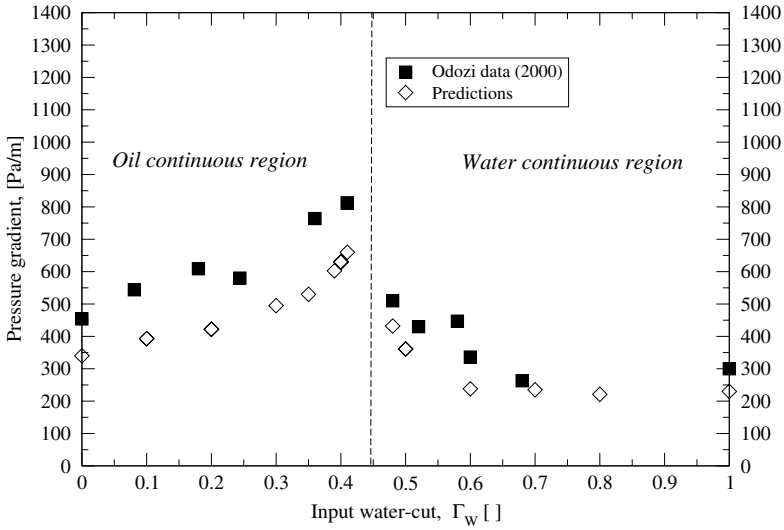

Fig. 12. Comparison between measured and predicted pressure gradients for Odozi three-phase slug flow test case.

water-cut of 0.2. On the other hand, the rate of change in pressure loss in the oil continuous region (from zero water-cut to phase inversion), and the abrupt drop across the phase inversion point, are both predicted with good accuracy.

The good agreement between experiments and predictions can be explained by the ability of the Decarre & Fabre model to capture the existence of turbulent or laminar dispersions locally, according to Eqs. (33) and (34). Indeed, in a previous study by Bonizzi (2003) the model of Brauner (2001) was implemented in place the Decarre & Fabre model. That model is restricted to turbulent flows only, and was found to give much less accurate predictions. The existence of laminar dispersions, which are catered for by the present model, typically leads to larger volumes of liquid dispersion in a slug unit (typically 50–70% in terms of total liquid volume, both in the oil and the water continuous regions, as shown in Fig. 13), especially when the continuous phase is a highly viscous oil. Ultimately, the enhanced value of effective viscosity (as predicted by the Brinkman viscosity model), can play an active role in triggering more slugs as the concentration of the dispersed phase increases. As the mixture viscosity increases, the shear between wall and liquid becomes larger, leading to an increase in average slug unit hold-up, as depicted in Fig. 14. It was found experimentally that as the water-cut goes from zero to higher values in the oil continuous region, the total hold-up increases, and reaches its peak close to the critical water fraction. After phase inversion, the hold-up decreases monotonically in the water-continuous region, and when $\Gamma_W = 1$ the value for air–water slug flow is eventually reached. The calculated trend is in fair agreement with the experiments: as phase inversion is approached, the global hold-up increases in the oil continuous region. After the inversion point, the lower mixture viscosity in the water-continuous region leads to smaller hold-ups. The good agreement found depends mainly on the liquid–liquid flow patterns that are allowed by the model. If segregation of oil and water had been excluded (i.e. by modelling the liquid field as a homogeneously dispersed oil–water mixture throughout the flow domain as done by Kempf, 2002), the results would not have led to the

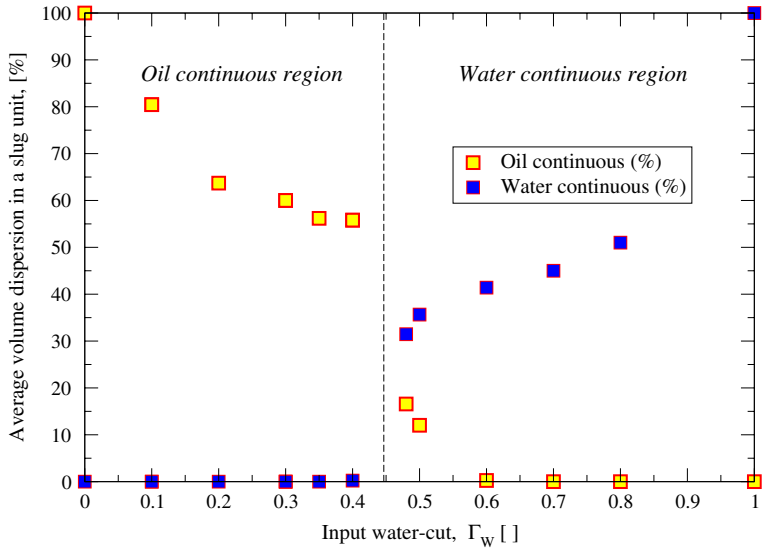

Fig. 13. Predicted average volumes of liquid dispersion in a slug unit for Odozi slug flow test case.

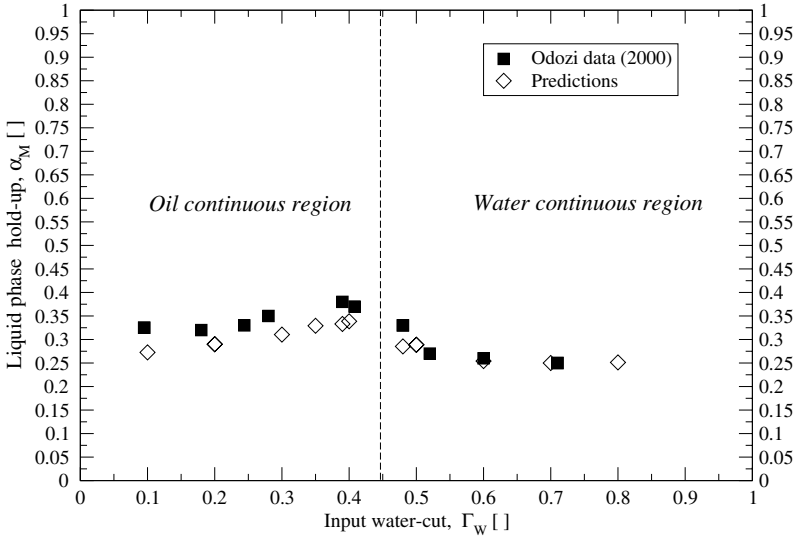

Fig. 14. Comparison between measured and predicted liquid hold-ups for Odozi three-phase slug flow test case.

correct slug characteristics, in particular the liquid mixture hold-up. Hence, it is crucial that stratification between the liquids is properly accounted for, with the related slip calculated from an appropriate model.

The slug frequency versus water-cut plot is presented in Fig. 15. In this case also, the agreement between experiments and predictions is quite good. In the oil continuous region, the calculated frequencies increase monotonically for water-cuts lower than 0.35; thereafter the peak value of

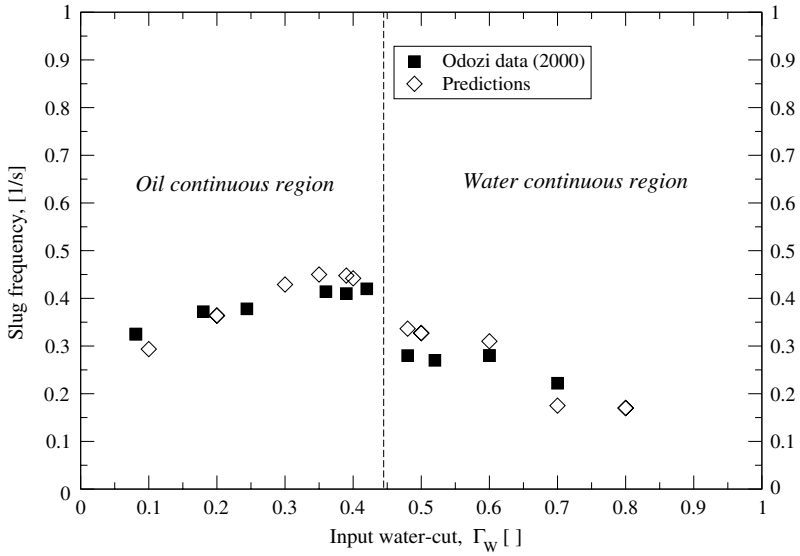

Fig. 15. Comparison between measured and predicted slug frequencies for Odozi three-phase slug flow test case.

0.45 1/s (with a discrepancy of just 7% with respect to the measurements) is maintained constant until phase inversion. When water becomes the continuous phase of the mixture, the frequencies gradually tend to lower values.

The second experiment considered for the assessment of the model is that of Stapelberg and Mewes (1994), who describe measurements of oil–water–air systems under slug flow conditions in a horizontal pipe 35 m long with an internal diameter of 0.059 m. The oil viscosity is 31×10^{-3} Pa s, with density of 858 kg/m^3. The oil–water surface tension was measured to be $\sigma_{OW} = 0.0535$ N/m. Compared to the physical properties of the liquids used by Odozi in his experiments, the oil–water viscosity ratio is lower (31 against 48), and the surface tension between the liquids is about 78% higher. In the experiments, for a fixed value of air velocity, the water fraction was varied in steps of 25% between 0 (two-phase air–oil flow) and 100% (two-phase air–water flow). The total liquid velocity was 0.244 m/s, except for the air–oil flow where a lower value (0.226 m/s) was used. The air velocity is varied in the range 0–3 m/s. The authors found that the flow pattern was slug for all gas and liquid flow rates, but unfortunately, they did not take into consideration, in the classification of the three-phase flow patterns, the level of dispersion between the liquids. They only state that, for low volume flow rates of the gas, the oil and water flow in a stratified state throughout the pipe, whereas, as the velocity of the air increases, the liquids start to mix in the slug body region. Regardless of the selected value of air volume rate, Stapelberg & Mewes did not find any peak in the slug characteristics (in particular pressure gradient and slug frequency) in the three-phase region. Instead, the measured pressure losses and slug frequencies were highest for the case of two-phase air and oil flow.

The calculations were carried out for a gas superficial velocity of $U_A = 2.5$ m/s. The calculations always predict slug flow, whether two or three-phase. Figs. 16 and 17 show the comparisons between predictions and measurements for pressure losses and slug frequencies respectively. In

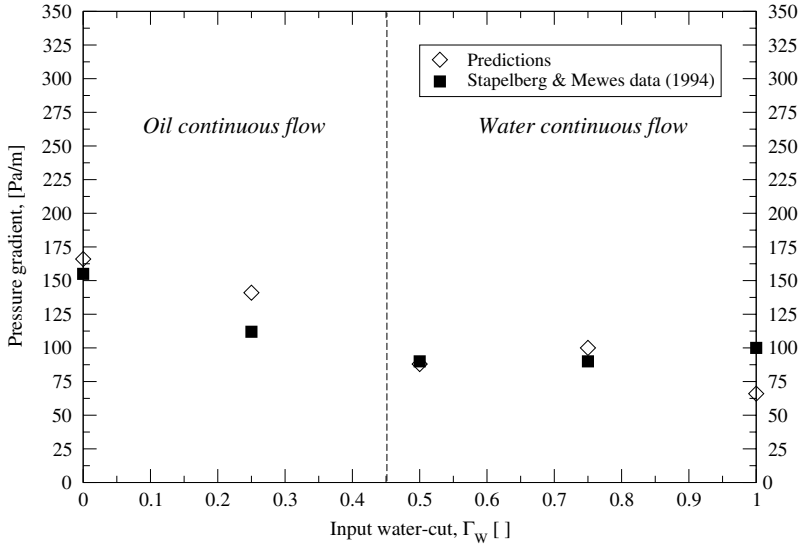

Fig. 16. Comparison between measured and predicted pressure gradients for Stapelberg & Mewes three-phase slug flow test case.

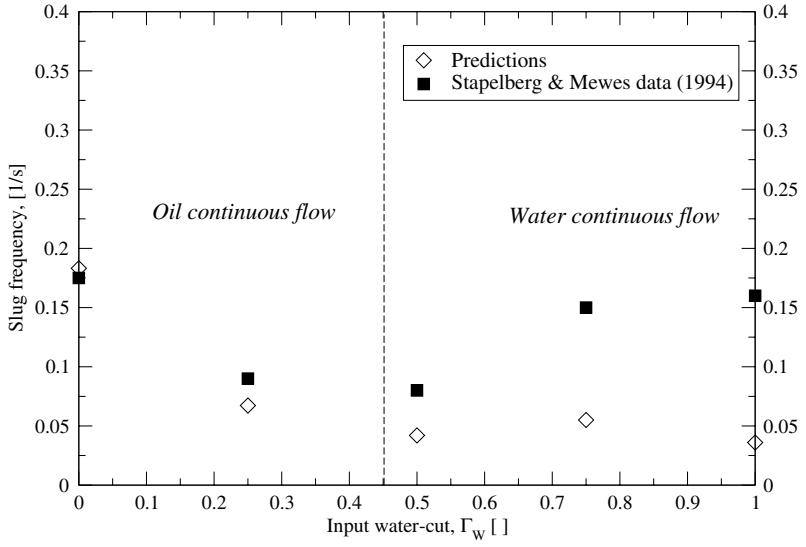

Fig. 17. Comparison between measured and predicted slug frequencies for Stapelberg & Mewes three-phase slug flow test case.

both figures the dashed line refers to the water fraction at which inversion occurs, according to the Decarre & Fabre model. The agreement between experiments and predictions in the oil continuous region is fairly good: the maximum pressure gradient occurs, as in the experiments, at a water-cut of 0%, corresponding to air–oil slug flow. As the water fraction increases, unlike in the

Odozi experiments, the pressure gradient diminishes. After the inversion point the pressure drop continues to decrease slightly, but then remain almost constant between $\Gamma_W = 0.5$ and 0.75. The average absolute discrepancy between experiment and prediction is 16%. Consistent with what happens to the pressure losses, the slug frequency is highest at the extreme of zero water flow. For a water-cut of 0.25, the predictions indicate a sharp decrease, similar to the measurements. The simulation, in fact, predicts longer slug sizes for that water-cut, implying that, on average, longer slug units will generate to carry the same liquid flow rate. In the water continuous region, the discrepancies between predictions and experiments become more evident as the water fraction is increased, although the two trends are similar. The absolute average discrepancy is 42%.

Although Stapelberg & Mewes do not report any measurement of the degree of dispersion between the liquid phases, the present predictions indicate that full dispersion always occurs in the slug body region; however, nearly the whole of the film is in the stratified oil–water flow pattern. When smaller portions of the slug unit are in the liquid–liquid dispersed flow regime, the enhanced mixture viscosity, as given by the Brinkman law (1952), cannot play a significant role as in the previous cases, where the liquids mix in much of the liquid film as well. The transition from liquid–liquid stratified to dispersed flow in the experiment of Stapelberg & Mewes is thus hindered due to the combination of high oil–water surface tension and low values of volumetric flow rates. These are thought to be responsible for the predicted trend (which is opposite to the previous one), a trend which is nonetheless still captured remarkably well by the model without any adjustment or tuning to the methodology.

5. Conclusions

A model to simulate three-phase (liquid/liquid/gas) slug flow in horizontal or nearly horizontal pipes has been developed based on the framework of the two-fluid model in conjunction with a drift–flux to combine the two sets of liquid equations into one. Hence the model could be easily implemented within an already existing two-phase slug flow simulator. Slugs are automatically captured from the solution of the conservation equations, provided that the mesh resolution is sufficiently fine.

The closure laws for the determination of the local liquid–liquid flow pattern, and the critical water fraction for the phase inversion, are crucial to the accuracy of the model. Two possible liquid–liquid flow patterns are catered for: either segregation, or full dispersion. The criterion adopted to discriminate between stratified and dispersed liquid–liquid flows is based on the prediction of the maximum drop size that generates under local flow conditions. If it is smaller than the critical size (above which dispersion cannot occur) the liquids are considered to be mixed; otherwise, they flow in separate layers. Furthermore, if dispersion occurs, a correlation is needed to determine which of the phases is continuous. The recommended closure is that by Decarre & Fabre, originally developed for the determination of the critical water fraction for phase inversion in a two-phase system. An interesting aspect of that model is that it caters for different types of flow regime (either laminar or turbulent) for each liquid phase, and takes into account the local flow conditions as well as the fluid properties. From the combinations of the possible liquid flow regimes (turbulent–turbulent, laminar–turbulent, or laminar–laminar), different relations are derived. In order to account for the increase in the dynamic viscosity of the mixture, a relation such

as that of Brinkman must be used. With the aforementioned models, good agreement between the numerical results and experimental data for the major slug characteristics was found.

It has to be remarked that although the model of Decarre & Fabre, performed extremely well in all the three-phase calculations discussed here, it is not valid for a wider spectrum of gas velocities. In fact, several experimental findings indicate that as the volumetric flow rate of the gas phase is increased, phase inversion would shift towards higher water-cuts. This physical effect seems to be due to gas entrainment that becomes greater as the gas velocity increases. Since Decarre & Fabre derived their model from studies of two-phase liquid–liquid pipe flow, it is evident that the equations would not account for the presence of gas bubbles in the dispersed liquid region. Also, the overall model presented here ignores the entrainment process (a feature which needs to be modelled in future). If accurate results are to be achieved regardless of the inlet gas flow rates, it is crucial for phase inversion in gas–liquid–liquid systems to be modelled better together with gas entrainment. The concept of modelling a spontaneous physical process, like phase inversion, using the criterion of minimisation of the total system energy appears to be most feasible; it has already been adopted successfully by Decarre and Fabre (1997), and by Brauner and Ullmann (2002), who both arrived at the same condition. Development of a more general model based on the same principles could provide a powerful tool in accounting for three-phase effects.

Acknowledgements

This work has been undertaken within the second stage of the Transient Multiphase Flows' Co-ordinated Research Project. The Authors wish to acknowledge the contributions made to this project by the Engineering and Physical Sciences Research Council (EPSRC) and to the following industrial organisations: ABB; AEA Technology; BG International; BP Exploration; Chevron; Conoco; Enterprise Oil; Granherne; Institutt for Energiteknikk; Institut Francais du Petrole; Marathon Oil; Mobil North Sea; Norsk Hydro; Scandpower; TotalFinaElf.

The authors also wish to thank Prof. G.F. Hewitt, his team and colleagues in the Department of Chemical Engineering at Imperial College, not only for the provision of experimental data, but also for the numerous discussions which had shed much light on the physics of three-phase slug flow.

References

Açikgöz, M., Franca, F., Lahey, R.T., 1992. An experimental study of three-phase flow regimes. Int. J. Multiphase Flow 18, 327–336.

Arirachakaran, S., Oglesby, K.D., Malinowsky, M.S., Shoham, O., Brill, J.P., 1989. An analysis of oil/water flow phenomena in horizontal pipes. SPE Paper 18836, pp. 155–187.

Banerjee, S., Chan, A.M.C., 1980. Separated flow models-I: analysis of the averaged and local instantaneous formulations. Int. J. Multiphase Flow 6, 1–24.

Barnea, D., 1986. Transition from annular flow and from dispersed bubble flow-unified models for the whole range of pipe inclinations. Int. J. Multiphase Flow 12, 733–744.

Barnea, D., Taitel, Y., 1996. Stratified three-phase flow in pipes-stability and transition. Chem. Eng. Comm. 141–142, 443–460.

Beggs, H.D., Brill, J.P., 1973. Study of two-phase flow in inclined pipes. J. Petr. Tech. 25, 607–617.

Bendiksen, K., Malnes, D., Moe, R., Nuland, S., 1991. The dynamic two-fluid model OLGA: theory and application. SPE Paper 19451, pp. 171–180.

Bonizzi, M., 2003. Transient one-dimensional modelling of multiphase slug flows. PhD Thesis, Imperial College, London, UK.

Brauner, N., Moalem Maron, D., 1992. Flow pattern transitions in two-phase liquid–liquid flow in horizontal tubes. Int. J. Multiphase Flow 18, 123–140.

Brauner, N., 2001. The prediction of dispersed flows boundaries in liquid–liquid and gas–liquid systems. Int. J. Multiphase Flow 27, 885–910.

Brauner, N., Ullmann, A., 2002. Modelling of phase inversion phenomenon in two-phase pipe flows. Int. J. Multiphase Flow 28, 1177–1204.

Brinkman, H.C., 1952. The viscosity of concentrated suspensions and solutions. J. Chem. Phys. 20, 571.

Decarre, S., Fabre, J., 1997. Etude sur la prediction de l'inversion de phase. Revue de l'Institut Français du Pétrole 52, 415–424.

Hale, C.P., Hewitt, G.F., 2001. Two-phase, gas–liquid transient experiments performed in a 1.5° downwardly inclined testline. Technical Report, Imperial College London, UK.

Hall, A.R.W., 1992. Multiphase flow of oil, water and gas in horizontal pipes. PhD Thesis, Imperial College London, UK.

Hall, A.R.W., 1997. Flow patterns in three-phase flows of oil, water and gas. In: 8th International Conference Multiphase Production, BHR Group Conference Series, Cannes, France.

Hand, N.P., 1991. Gas–liquid co-current flow in a horizontal pipe. PhD Thesis, Queen's University, Belfast.

Hinch, E.J., Acrivos, A., 1979. Steady long slender droplets in two-dimensional straining motion. J. Fluid Mech. 91, 401–414.

Hinze, J., 1955. Fundamentals of the hydrodynamic mechanism of splitting in dispersion processes. J. AIChE 3, 289–295.

Hirsch, C., 1988. Numerical Computation of Internal and External Flows. John Wiley & Sons, New York. p. 1.

Ishii, M., 1978. One-dimensional drift–flux model and constitutive equations for relative motion between phases in various two-phase flow regimes. Technical Report ANL-77-47, Argonne National Laboratory, Argonne, Illinois, US.

Issa, R.I., Woodburn, P.J., 1998. Numerical prediction of instabilities and slug formation in horizontal two-phase flows. In: 3rd International Conference Multiphase Flow, ICMF98, Lyon, France.

Issa, R.I., Kempf, M.H.W., 2003. Simulation of slug flow in horizontal or nearly horizontal pipes with the two-fluid model. Int. J. Multiphase Flow 29, 69–95.

Kempf, M.H.W., 2002. Simulation of three-phase slug flow using the two-fluid model with a mixture viscosity. Technical Report, Imperial College, London, UK.

Khor, S.H., Mendes-Tatsis, M.A., Hewitt, G.F., 1997. One-dimensional modelling of phase holdups in three-phase stratified flow. Int. J. Multiphase Flow 23, 885–897.

Larsen, M., Hustvedt, E., Hedne, P., Straume, T., 1997. Petra: a novel computer code for simulation of slug flow. SPE Paper 38841, pp. 965–976.

Larsen, M., Hedne, P., 2001. Three-phase slug tracking with Petra. In: Proceedings of ETCE2001 Eng. Techn. Conf. On Energy, Houston, Texas, US.

Malinowsky, M.S., 1975. An experimental study of oil–water and air–oil–water flowing mixtures in horizontal pipes. MS Thesis, The University of Tulsa, US.

Nädler, M., Mewes, D., 1995. Intermittent three-phase flow of oil, water and gas in horizontal pipes. In: Proceedings of 5th International Offshore and Polar Eng. Conference, The Hague, The Netherlands.

Nydal, O.J., Banerjee, S., 1996. Dynamic slug tracking simulations for gas–liquid flow in pipelines. Chem. Eng. Comm. 141–142, 13–39.

Odozi, U.A., 2000. Three-phase gas/liquid/liquid slug flow. PhD Thesis, Imperial College, London, UK.

Odozi, U.A., Mendes-Tatsis, M.A., Hewitt, G.F., 1998. Pressure drop and liquid holdup in threephase air–oil–water slug flow. In: 3rd International Conference Multiphase Flow, ICMF 98, Lyon, France.

Pan, L., 1996. High pressure three-phase (gas/liquid/liquid) flow. PhD Thesis, Imperial College, London, UK.

Pauchon, C., Dhulesia, H., Binh-Cirlot, G., Fabrem, J., 1994. Tacite: a transient tool for multiphase pipeline and well simulation. In: SPE Annual Technical Conference and Exhibition, SPE Paper 28545, New Orleans, LA, US.

Stapelberg, H.H., Mewes, D., 1994. The pressure loss and slug frequency of liquid–liquid–gas slug flow in horizontal pipes. Int. J. Multiphase Flow 20, 285–303.

Taitel, Y., Barnea, D., Brill, J.P., 1995. Stratified three phase flow in pipes. Int. J. Multiphase Flow 21, 53–60.

Taitel, Y., Barnea, D., 1998. Effect of gas compressibility on a slug tracking model. Chem. Eng. Sci. 53, 2089–2097.

Utvik, O.H., Valle, A., RINDE, T., 1998. Pressure drop, flow pattern and slip for a multiphase crude oil–water-hydrocarbon gas system. In: 3rd International Conference Multiphase Flow, ICMF98, Lyon, France.

Valle, A., 1998. Multiphase pipeline flows in hydrocarbon recovery. Multiphase Sci. Tech. 10, 1–139.

Zheng, G., Brill, J.P., Taitel, Y., 1994. Slug flow behaviour in a hilly terrain pipeline. Int. J. Multiphase Flow 20, 63–79.